 CMES, vol.23, no.2, pp.127-147, 2008

# A Hybrid Multi-Region BEM / LBIE-RBF Velocity-Vorticity Scheme for the Two-Dimensional Navier-Stokes Equations

**E.J. Sellountos**[1] **and A. Sequeira** [1]

**Abstract:** In this work a hybrid velocity-vorticity scheme for the solution of the 2D Navier-Stokes equations is presented. The multi-region Local Boundary Integral Equation (LBIE) combined with Radial Basis Functions (RBF) interpolation is used for the solution of the kinematics and the multi-region BEM for the solution of the transport kinetics. The final system of equations is in band form for both methods. The issue of RBF discontinuities is resolved by constructing the RBF matrix locally in every region. The kinematics integral equation is used in three different forms, for coupling the velocity field on the boundary, on interior points and on points belonging to interfaces. The convective velocity is decomposed into a constant and a variable part, and the constant part is a term of the parabolic-diffusion fundamental solution resulting on a very effective upwind technique for the transport kinetics. The complete absence of the derivatives and the same nodal discretization for both equations give a very strong coupling between the kinematics and the kinetics.

**Keyword:** Local Boundary Integral Equation (LBIE), Boundary Elements Method (BEM) Navier-Stokes, Radial Basis Functions (RBF), RBF discontinuity, velocity-vorticity.

## 1 Introduction

The Navier-Stokes equations are often solved using the velocity-vorticity formulation. The pressure gradient is eliminated from the governing equations leading to the numerical separation of the kinematics and kinetics aspects of the fluid flow [Skerget and Rek (1995), Liu (2001), Zhu (2005) and Nicolás and Bermúdez (2007)]. The pressure can be post-processed after obtaining the solution for velocity and vorticity.

The BEM is a well established numerical technique for solving the Navier-Stokes equations using the velocity-vorticity formulation [Skerget, Hribersek, and Zunic (2003) and Hribersek and Skerget (2005)]. The accurate integral equations of the kinematics related to the mass conservation, the complete absence of the derivatives in the computation and the usage of the convective parabolic-diffusion fundamental solution results in a very accurate, robust and stable tool in CFD. The most interesting issue in the conservation integral equation is the absence of the velocity flux and the strong coupling it provides between velocity and vorticity [Zunic, Hribersek, Skerget, and Ravnik (2007)].

On the other hand, several mesh-reduction techniques have been developed in the literature known mainly as "meshless" methods and they are used for the solution of the Navier-Stokes equations, see e.g. [Lin and Atluri (2001)], [Onate, Idelsohn, Zienkiewicz, and Taylor (1998)], [Wu, Tsay, and Young (2005)], [Tsai, Young, and Cheng (2002)] [Cheng and Liu (2002)] and [Shu, Ding, and Yeo (2005)]. The LBIE is based on the BEM integral equations and is considered as the free-mesh BEM formulation (see e.g. [Sellountos and Polyzos (2003)]). Since LBIE is closely related to BEM, their coupling is straightforward ([Sellountos and Polyzos (2005)]). In the present work however the LBIE is combined with BEM for the solution of the Navier-Stokes equations. Recently in the work [Sellountos and Sequeira (2007)] the LBIE was used for the solution of incompresible fluid flows by adopting the velocity-vorticity formu-

[1] Department of Mathematics and CEMAT, Instituto Superior Técnico, Technical University of Lisbon, Av. Rovisco Pais, 1, 1049-001, Lisbon, Portugal.

lation. The conservation equations as they are presented in [Hribersek and Skerget (2005)], are solved locally by the LBIE combining three different forms of the kinematics, the tangential and the normal form for boundary points and the regular form for the interior points. The interpolation of the unknown field is accomplished by associating every nodal point with an RBF matrix. In this way the computation of integrals is very fast and the matrices associated to the final system of equations are banded with narrow bandwidth resulting in a fast iteration process. Although both of them are essential for CFD methods, the notorious issue of "equally spaced points" still remains and the reason of that is the discontinuitity and the incompatibility of the RBF interpolation [Liu, Gu, and Dai (2004)] when the nodal points are non-uniformly distributed. In the present work this issue is circumvented by the multi-region approach. Every region is associated with an RBF matrix, which is inverted only once leading again to a fast computation of integrals. Since RBF satisfy the delta property, the imposition of the boundary conditions is simple and straightforward. The lid-driven cavity is a typical example where non-uniformly distributed points must be used.

Moreover further development have been made in the coupling of the kinematics integral equations. The regular form of the kinematics and the continuity conditions are applied on the interfacial nodal points. This ensures the continuity of the velocity in the entire domain, and results band form of kinematics systems of equations.

On the other hand the multi-region BEM [Hribersek and Skerget (1998)] is adopted for the solution of the transport kinetics equation, exploiting the effective upwind scheme provided by the convective parabolic-diffusion integral equation. In the present work discontinuous boundary elements and special discontinuous RBF cells are used.

The paper is organized as follows: in section 2 the integral equations for the velocity and vorticity field are presented for both the LBIE kinematics and the BEM transport kinetics. In section 3 the RBF interpolation used in the present multi-region scheme is presented. In section 4 some technical details about the scheme are addressed and the discretized form of the integral equations are given. Finally in section 5 three representative examples are solved.

## 2 Integral equations

The set of governing equations that describe the flow of an incompressible fluid includes the conservation of mass and the conservation of momentum [Zienkiewicz and Taylor (2000)].

$$\nabla \cdot \mathbf{u} = 0 \tag{1}$$

$$\frac{\partial \mathbf{u}}{\partial t} + \mathbf{u} \cdot \nabla \mathbf{u} = -\frac{1}{\rho} \nabla P + \nu \nabla^2 \mathbf{u}. \tag{2}$$

In the above equations, $\mathbf{u}$ is the velocity vector, $P$ is the pressure, $\rho$ the density and $\nu$ is the diffusion coefficient or viscosity. It is well known [Hribersek and Skerget (2005)] that numerical methods based on the weak formulations of Eq. 1 and Eq. 2 have numerical instabilities related to the presence of the pressure gradient term. This term can be circumvented by adopting the velocity-vorticity formulation, which is obtained by applying the curl operator in both Eq. 1 and Eq. 2, i.e.

$$\nabla^2 \mathbf{u} + \nabla \times \omega = \mathbf{0} \tag{3}$$

$$\frac{\partial \omega}{\partial t} + \mathbf{u} \cdot \nabla \omega - \omega \cdot \nabla \mathbf{u} - \nu \nabla^2 \omega = \mathbf{0} \tag{4}$$

where $\omega$ is the vorticity vector which is defined as

$$\omega = \nabla \times \mathbf{u}. \tag{5}$$

In two-dimensional fluid flows, the vorticity has only one component perpedicular to the plane of the flow ($\omega \cdot \nabla \mathbf{u} = \mathbf{0}$) and therefore the Eq. 3 and Eq. 4 can be written in the following simplified form

$$\frac{\partial^2 u_i}{\partial x_j \partial x_j} + e_{ij} \frac{\partial \omega}{\partial x_j} = 0 \tag{6}$$

$$\frac{\partial \omega}{\partial t} + u_j \frac{\partial \omega}{\partial x_j} - \nu \frac{\partial^2 \omega}{\partial x_j^2} = 0. \tag{7}$$

The coupled Eq. 6 and Eq. 7, known as velocity-vorticity formulation [Guj and Stella (1993)] of

the Navier-Stokes equations Eq. 1 and Eq. 2, represent the kinematic and the kinetic dynamics of an incompressible Newtonian fluid. The corresponding initial boundary value problem must be complemented with the initial conditions

$$\begin{aligned} u_i(\mathbf{x},0) &= u_i^{(0)} \\ \omega_i(\mathbf{x},0) &= \omega_i^{(0)} \end{aligned} \quad \text{for } \mathbf{x} \in \Gamma \tag{8}$$

and one of the following boundary conditions

$$\begin{aligned} u_i(\mathbf{x},t) &= \overline{u}_i \\ \omega_i(\mathbf{x},t) &= \overline{\omega}_i \end{aligned} \quad \text{for } \mathbf{x} \in \Gamma. \tag{9}$$

### 2.1 Local integral equations for flow kinematics

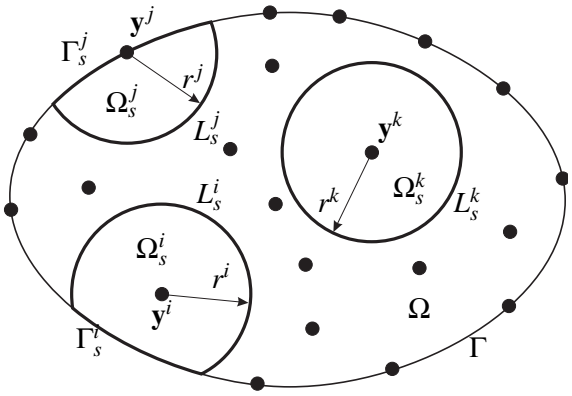


Figure 1: Local support domains $r$, boundary segments $\Gamma_s$, local circular surfaces $L_s$ and local volumes $\Omega_s$.

For a 2D domain $\Omega$ bounded by a smooth boundary $\Gamma$, the flow of an incompressible Newtonian fluid (Fig. 1) described by Eq. 6-Eq. 7 with the initial and boundary conditions Eq. 8-Eq. 9 form a well posed boundary value problem which admits the following boundary-domain integral representation [Skerget, Hribersek, and Zunic (2003)]:

$$\begin{aligned} c(\mathbf{y})\mathbf{u}(\mathbf{y}) + \int_\Gamma (\nabla u^* \cdot \mathbf{n})\,\mathbf{u}\,d\Gamma = \\ \int_\Gamma (\nabla u^* \times \mathbf{n}) \times \mathbf{u}\,d\Gamma + \\ \int_\Omega (\omega \times \nabla u^*)\,d\Omega. \end{aligned} \tag{10}$$

Here $\mathbf{c}$ is a jump coefficient being equal to 1 for interior points and equal to 0.5 for points belonging to the smooth boundary $\Gamma$ and $u^*$ is the fundamental solution of the Laplace operator having the following form

$$u^* = \frac{1}{2\pi}\mathrm{Log}\left(\frac{1}{r}\right) \tag{11}$$

with $r = |\mathbf{y} - \mathbf{x}|$ representing the distance between the reference point $\mathbf{y}$ and the source point $\mathbf{x}$ and $\mathbf{n}$ denoting the outward unit vector normal to the boundary. It is obvious that the fundamental solution given by Eq. 11 becomes singular only when the field point $\mathbf{y}$ coincides with the source point $\mathbf{x}$. Thus, considering a local circular sub-domain $\Omega_s$ with boundary $L_s$ centered at point $\mathbf{y}$ and applying the Green's integral identity in the domain lying between the global and local boundaries $\Gamma$ and $L_s$, respectively, it is easy to see that Eq. 10 can be replaced by the following local boundary-volume integral equation

$$\begin{aligned} c(\mathbf{y})\mathbf{u}(\mathbf{y}) + \int_{\Gamma_s \cup L_s} (\nabla u^* \cdot \mathbf{n})\,\mathbf{u}\,d\Gamma = \\ \int_{\Gamma_s \cup L_s} (\nabla u^* \times \mathbf{n}) \times \mathbf{u}\,d\Gamma + \\ \int_{\Omega_s} (\omega \times \nabla u^*)\,d\Omega \end{aligned} \tag{12}$$

where $\Gamma_s$ is part of the global boundary intersected with the local sub-domain $\Omega_s$, as illustrated in Fig. 1. In addition with Eq. 12 two equivalent integral equations for boundary points are considered. The first one is the tangential form ([Hribersek and Skerget (2005)] and [Alujevic, Kuhn, and Skerget (1991)])

$$\begin{aligned} c(\mathbf{y})\mathbf{n}(\mathbf{y}) \times \mathbf{u}(\mathbf{y}) + \mathbf{n}(\mathbf{y}) \times \int_{\Gamma_s \cup L_s} (\nabla u^* \cdot \mathbf{n})\,\mathbf{u}\,d\Gamma = \\ \mathbf{n}(\mathbf{y}) \times \int_{\Gamma_s \cup L_s} (\nabla u^* \times \mathbf{n}) \times \mathbf{u} d\Gamma + \\ \mathbf{n}(\mathbf{y}) \times \int_{\Omega_s} (\omega \times \nabla u^*)\,d\Gamma \end{aligned} \tag{13}$$

and the second one is the following normal form

$$c(\mathbf{y})\mathbf{n}(\mathbf{y})\cdot\mathbf{u}+\mathbf{n}(\mathbf{y})\cdot\int_{\Gamma_s\cup L_s}(\nabla u^*\cdot\mathbf{n})\,\mathbf{u}\,d\Gamma= \mathbf{n}(\mathbf{y})\cdot\int_{\Gamma_s\cup L_s}(\nabla u^*\times\mathbf{n})\times\mathbf{u}\,d\Gamma+ \mathbf{n}(\mathbf{y})\cdot\int_{\Omega_s}(\omega\times\nabla u^*)\,d\Gamma. \quad (14)$$

In the present work the set of Eq. 12 Eq. 13 Eq. 14 will be coupled and solved by the LBIE.

### 2.2 *Boundary domain integral equations for flow kinetics*

Since the first time derivative of the vorticity appears in Eq. 7, it is very convenient to employ the finite differences scheme

$$\frac{\partial\omega}{\partial t}=\frac{\omega-\omega_{t-1}}{\Delta t} \quad (15)$$

where $\omega_{t-1}$ is the vorticity field at the previous time step and $\Delta t$ is the considered time step. The convective velocity is decomposed into a constant and a variable part

$$\mathbf{u}=\overline{\mathbf{u}}+\tilde{\mathbf{u}} \quad (16)$$

In view of Eq. 15 and Eq. 16, Eq. 7 takes the following form

$$\frac{\partial^2\omega}{\partial x_j^2}-\frac{1}{\nu}\overline{u}_j\frac{\partial\omega}{\partial x_j}-\frac{1}{\nu}\frac{\omega}{\Delta t}+\left(-\frac{1}{\nu}\tilde{u}_j\frac{\partial\omega}{\partial x_j}+\frac{1}{\nu}\frac{\omega_{t-1}}{\Delta t}\right)=0 \quad (17)$$

or

$$\frac{\partial^2\omega}{\partial x_j^2}-\frac{1}{\nu}\overline{u}_j\frac{\partial\omega}{\partial x_j}-\frac{1}{\nu}\frac{\omega}{\Delta t}+b=0 \quad (18)$$

where $b$ represents the body forces

$$b=-\frac{1}{\nu}\tilde{u}_j\frac{\partial\omega}{\partial x_j}+\frac{1}{\nu}\frac{\omega_{t-1}}{\Delta t}. \quad (19)$$

Exploiting the diffusion-convection fundamental solution (see [Hribersek and Skerget (2005)] and [Bokota and Iskierka (1995)])

$$p^*=\frac{1}{2\pi}K_0(\mu r)\exp\left(\frac{\overline{\mathbf{u}}\cdot\mathbf{r}}{2\nu}\right) \quad (20)$$

where

$$\mu=\sqrt{\left(\frac{|\overline{\mathbf{u}}|}{2\nu}\right)^2+\beta}$$
$$\beta=\frac{1}{\nu\Delta t} \quad (21)$$

with $\mathbf{r}=\mathbf{y}-\mathbf{x}$, and applying the Green's second identity for the scalars $p^*$ and $\omega$, one obtains the following integral equation:

$$c(\mathbf{y})\,\omega(\mathbf{y})+\int_\Gamma\frac{\partial p^*}{\partial n}\omega\,d\Gamma= \int_\Gamma p^*\left(\frac{\partial\omega}{\partial n}-\frac{1}{\nu}u_n\omega\right)d\Gamma+ \frac{1}{\nu}\int_\Omega\frac{\partial p^*}{\partial x_j}\tilde{u}_j\omega\,d\Omega+ \frac{1}{\nu\Delta t}\int_\Omega p^*\omega_{t-1}\,d\Omega \quad (22)$$

where $u_n=\mathbf{u}\cdot\mathbf{n}$. In the present hybrid scheme the transport boundary-domain integral equation Eq. 22 will be solved by the BEM.

## 3 Radial Basis Functions Interpolation

In this section an interpolation scheme based on the RBFs is proposed and illustrated [Li, Hon, and Chen (2002), Wang and Liu (2002a)]. The RBFs are used for the interpolation of the velocity in the kinematics as well as for the interpolation of the vorticity on special discontinuous cell elements in the kinetics. As it is already known the RBFs satisfy the delta property and hence the imposition of the boundary conditions is straightforward. Moreover the inverse matrix depends only on the relative placement of the nearby nodal points [Atluri and Shen (2002)] and thus it is computed only once. Both characteristics are very important since they accelerate the computation of the boundary and volume integrals. For the kinematics a closed domain, as that shown in Fig. 2 (a), is divided into a number of regions and every region is further discretized into $N$ boundary and interior nodal points. Each nodal point $\mathbf{y}_j$ is placed in the center of a circular domain with radius $r_j$ which is called support domain of $\mathbf{y}_j$. The interface nodal points are involved in the interpolation, independently for every region. For the ki-

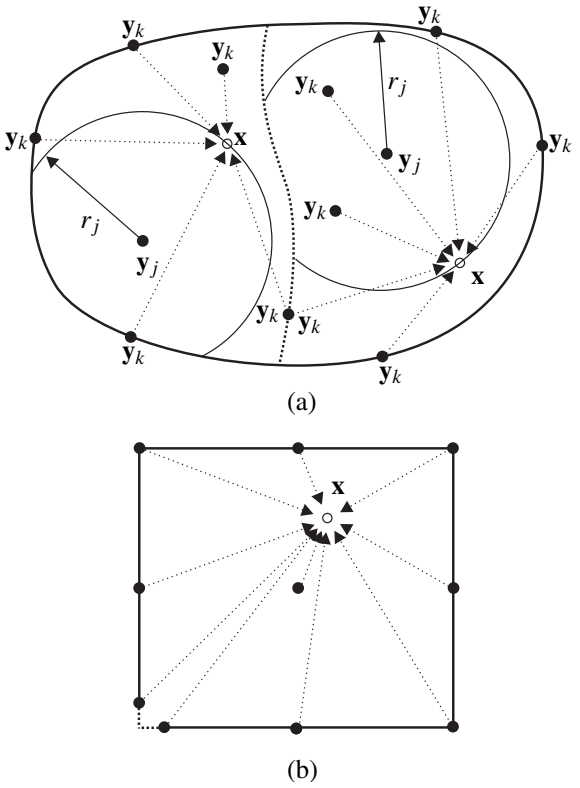


Figure 2: (a) Independent interpolation of the velocity field in two regions at integration points $\mathbf{x}$ and (b) special discontinuous RBF cell element.

netics cell elements Fig. 2 (b) the same consideration is being made where $N$ nodal points in a proper arrangement form a discontinuous quadrature cell element. At any point $\mathbf{x}$, the interpolation of an unknown field is accomplished by the following relation [Wang and Liu (2002b)]

$$u(\mathbf{x}) = \sum_{i=1}^{N} B_i a_i + \sum_{l=1}^{m} P_l b_l = \mathbf{B}^T(\mathbf{y}_k, \mathbf{x})\mathbf{a}(\mathbf{y}_k) + \mathbf{P}^T(\mathbf{x})\mathbf{b}(\mathbf{y}_k). \tag{23}$$

where $N$ is the total number of the nodal points belonging to the kinematics region or the total number of points belonging to the kinetics cell and $m$ is the degree of the polynomial basis used for the interpolation. For linear basis, $m$ is equal to 3, while for quadratic basis, $m$ is equal to 6. $\mathbf{B}(\mathbf{y}_k, \mathbf{x})$ is the RBF vector with dimension $N \times 1$ that links every nodal point $\mathbf{y}_k$ $k = 1, .., N$ with the point $\mathbf{x}$. $\mathbf{a}(\mathbf{y}_k)$ and $\mathbf{b}(\mathbf{y}_k)$ are unknown vectors with dimensions $N \times 1$ and $m \times 1$, respectively, that depend on the relative location of the nodal points $\mathbf{y}_k$. Finally, $\mathbf{P}(\mathbf{x})$ stands for a monomial basis vector with dimension $m \times 1$. More precisely, the vector $\mathbf{B}(\mathbf{y}_k, \mathbf{x})$ has the form

$$\mathbf{B}(\mathbf{y}_k, \mathbf{x}) = \begin{bmatrix} W(\mathbf{y}_1, \mathbf{x}) \\ W(\mathbf{y}_2, \mathbf{x}) \\ \cdots \\ W(\mathbf{y}_k, \mathbf{x}) \end{bmatrix}_{N \times 1}, \qquad k = 1, .., N \tag{24}$$

where $W$ represents a prescribed radial function. For linear basis, the polynomial vector $\mathbf{P}$ has the following form

$$\mathbf{P}^T(\mathbf{x}) = \begin{bmatrix} 1 & x & y \end{bmatrix}_{1 \times m} \tag{25}$$

while, for quadratic basis is written as

$$\mathbf{P}^T(\mathbf{x}) = \begin{bmatrix} 1 & x & y & x^2 & xy & y^2 \end{bmatrix}_{1 \times m}. \tag{26}$$

The determination of the unknown vectors $\mathbf{a}(\mathbf{y}_k)$ and $\mathbf{b}(\mathbf{y}_k)$ is accomplished by constructing a set of equations that relate each other the nodal points $\mathbf{y}_k$ used for the interpolation

$$u(\mathbf{y}_e) = \sum_{k=1}^{N} B_k(\mathbf{y}_k, \mathbf{y}_e) a_k(\mathbf{y}_k) + \sum_{l=1}^{m} P_l(\mathbf{y}_e) b_l(\mathbf{y}_e) \tag{27}$$

where $\mathbf{y}_e, e = 1, ..., N$ are also the interpolation nodal points. In addition to the previous relation the following equation is taken into account [Wang and Liu (2002a)]

$$\sum_{k=1}^{N} P_l(\mathbf{y}_k) a_k(\mathbf{y}_k) = 0, \qquad l = 1, .., m \tag{28}$$

and the following system of equations is formed

$$\begin{bmatrix} \mathbf{B_0} & \mathbf{P_0} \\ \mathbf{P_0}^T & \mathbf{0} \end{bmatrix}_{(N+m)\times(N+m)} \begin{bmatrix} \mathbf{a} \\ \mathbf{b} \end{bmatrix}_{N+m} = \begin{bmatrix} \mathbf{u} \\ \mathbf{0} \end{bmatrix}_{N+m} \tag{29}$$

or

$$\mathbf{A}(\mathbf{y}_k) \begin{bmatrix} \mathbf{a} \\ \mathbf{b} \end{bmatrix} = \begin{bmatrix} \mathbf{u} \\ \mathbf{0} \end{bmatrix}. \tag{30}$$

The matrix $\mathbf{A}(\mathbf{y}_k)$ is symmetric and consists of the submatrices $\mathbf{B}_0(\mathbf{y}_k,\mathbf{y}_e)$ and $\mathbf{P}_0(\mathbf{y}_e)$ that depend on the nodal points $\mathbf{y}_k$, $\mathbf{y}_e$ and have the following form

$$\mathbf{B}_0(\mathbf{y}_k,\mathbf{y}_e)=\left[\begin{array}{c}\mathbf{B}^T(\mathbf{y}_k,\mathbf{y}_1)\\ \mathbf{B}^T(\mathbf{y}_k,\mathbf{y}_2)\\ \cdots\\ \mathbf{B}^T(\mathbf{y}_k,\mathbf{y}_N)\end{array}\right]_{N\times N} \tag{31}$$

or

$$\mathbf{B}_0=\left[\begin{array}{cccc}W(\mathbf{y}_1,\mathbf{y}_1) & W(\mathbf{y}_2,\mathbf{y}_1) & \cdots & W(\mathbf{y}_N,\mathbf{y}_1)\\ W(\mathbf{y}_1,\mathbf{y}_2) & W(\mathbf{y}_2,\mathbf{y}_2) & \cdots & W(\mathbf{y}_N,\mathbf{y}_2)\\ \cdots & \cdots & \cdots & \cdots\\ W(\mathbf{y}_1,\mathbf{y}_N) & W(\mathbf{y}_2,\mathbf{y}_N) & \cdots & W(\mathbf{y}_N,\mathbf{y}_N)\end{array}\right]_{N\times N} \tag{32}$$

and

$$\mathbf{P}_0(\mathbf{y}_k)=\left[\begin{array}{c}\mathbf{P}^T(\mathbf{y}_1)\\ \mathbf{P}^T(\mathbf{y}_2)\\ \cdots\\ \mathbf{P}^T(\mathbf{y}_N)\end{array}\right]_{N\times m}. \tag{33}$$

Finally Eq. 23 is written in the form

$$\begin{aligned}u(\mathbf{x})=&\left[\begin{array}{cc}\mathbf{B}^T(\mathbf{y}_k,\mathbf{x}) & \mathbf{P}^T(\mathbf{x})\end{array}\right]\mathbf{A}^{-1}(\mathbf{y}_k)\left[\begin{array}{c}\mathbf{u}(\mathbf{y}_k)\\ \mathbf{0}\end{array}\right]\\ =&\mathbf{\Phi}(\mathbf{x},\mathbf{y}_k)\,\mathbf{u}(\mathbf{y}_k)\end{aligned} \tag{34}$$

with

$$\begin{aligned}\phi^k(\mathbf{x})=&\sum_{i=1}^{N}B_i(\mathbf{y}_i,\mathbf{x})A_{i,k}^{-1}(\mathbf{y}_k)+\\ &\sum_{l=1}^{m}P_l(\mathbf{x})A_{n+l,k}^{-1}(\mathbf{y}_k)\end{aligned} \tag{35}$$

representing the interpolation functions adopted in the present work. The derivatives of the interpolation functions can be derived by differentiating Eq. 35 with respect to the spatial coordinates $x,y$

$$\begin{aligned}\frac{\partial\phi^k(\mathbf{x})}{\partial x_1}=&\sum_{i=1}^{N}\frac{\partial B_i(\mathbf{y}_i,\mathbf{x})}{\partial x_1}A_{i,k}^{-1}(\mathbf{y}_k)+\\ &\sum_{l=1}^{m}\frac{\partial P_l(\mathbf{x})}{\partial x_1}A_{N+l,k}^{-1}(\mathbf{y}_k)\\ \frac{\partial\phi^k(\mathbf{x})}{\partial x_2}=&\sum_{i=1}^{N}\frac{\partial B_i(\mathbf{y}_i,\mathbf{x})}{\partial x_2}A_{i,k}^{-1}(\mathbf{y}_k)+\\ &\sum_{l=1}^{m}\frac{\partial P_l(\mathbf{x})}{\partial x_2}A_{N+l,k}^{-1}(\mathbf{y}_k).\end{aligned} \tag{36}$$

Multiquadric radial functions are employed in the present paper, i.e.

$$W(\mathbf{y},\mathbf{x})=\left(r^2+R^2\right)^{0.5} \tag{37}$$

where $r=|\mathbf{y}-\mathbf{x}|$ is the distance between the two points and R is a nodal parameter, the optimal value of which is determined to be equal to (see [Hardy (1990)])

$$R(\mathbf{y}_k)=0.815\frac{1}{N}\sum_{i=1}^{N}d_i \tag{38}$$

where $d_i$ is the distance between the $i$-th nodal point $\mathbf{y}_i$ and its closest nodal point. The partial derivatives of the weight function are given by

$$\frac{\partial W(\mathbf{y},\mathbf{x})}{\partial x_i}=-r_i\left(r^2+R^2\right)^{-0.5} \tag{39}$$

where $r_i$ is the $i$-th component of the vector $\mathbf{r}=\mathbf{y}-\mathbf{x}$.

## 4 Discretization and numerical implementation

### *4.1 Discretization of the domain*

The double discretization of the entire domain into a number of regions as shown in Fig. 3 is essential for the following reasons. In the case of the LBIE/RBF approach used for the kinematics, the maintenance of the locality is important. However the issue of incompatibility [Liu, Gu, and Dai (2004)] and discontinuity of the RBF interpolation is a major problem for non-uniform distributed nodal points when the RBFs are used

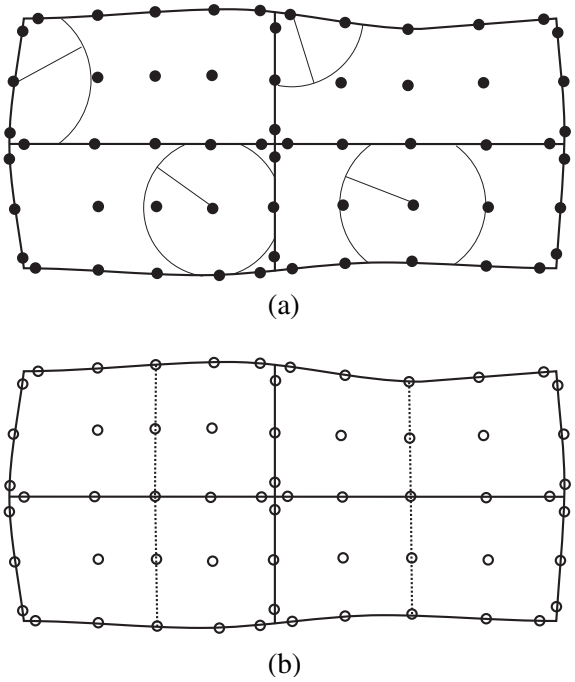


Figure 3: Double discretization for (a) LBIE kinematics and (b) BEM kinetics.

locally. This problem is circumvented by associating every region to an RBF matrix as it is explained in section 3. Extensive numerical testing showed that one region should contain the minimum possible number of nodal points, but for the sake of generality it can contain any number of points. If the region contains too many points, the inversion of the RBF matrix in Eq. 30 is computationally expensive and the evaluation of the interpolation functions in Eq. 35 eventually will be slower, bringing more computational cost in the evaluation of the integrals. In Fig. 3 (a) the RBF interpolation is guaranteed to be continuous in all the four regions.

For the kinetics the discretization of the domain into a number of regions as shown in Fig. 3 (b) is important due to the following reasons. First the integral equation Eq. 22 produces fully populated matrices and the solution is very time consuming. With the multi-region technique [Hribersek and Skerget (2005)] the system of equations has a sparse structure and after an apropriate positioning it takes band form. The solution is obtained faster and this leads to a significantly faster iteration process. Moreover every region is associated with a constant part of the convective velocity Eq. 16. As more of the convective term could be expressed through the constant part of the velocity the better the transport equation would behave. For the kinetics, discontinuous elements are used when it is necessary, i.e. in corner points. The RBF cell elements have the form of Fig. 4 and they can have a variable number of nodal points. The arrangement of the nodal points is such that

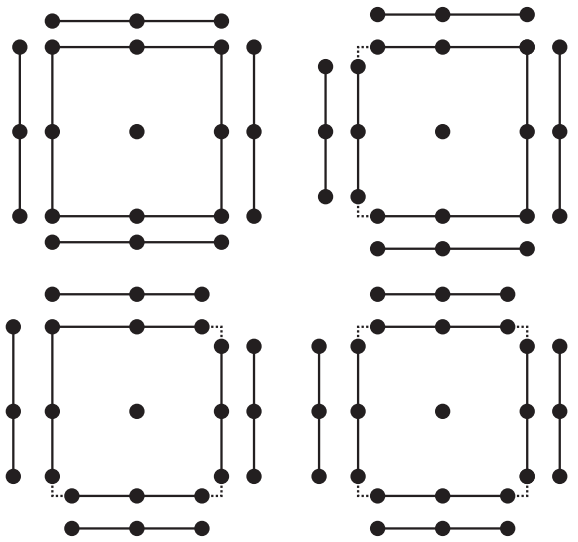

Figure 4: Continuous and various types of discontinuous RBF cells bounded by discontinuous boundary elements.

every kinetics nodal point matches with one kinematics nodal point. Discontinuous boundary elements have the same shape as the walls of the discontinuous RBF cells and so every discontinuous boundary node matches with the discontinuous RBF cell node as shown in Fig. 3. Under this consideration the system of equations is balanced with the same number of equations and unknowns.

### *4.2 Kinematics integral equation*

In the present formulation the kinematics system of equations consists of unknown veloci-

ties defined on boundary, interior and interfacial points and unknown vorticities defined only on the boundary points where the velocity is prescribed. The primary goal of the kinematics system of equations is to solve the velocity field. In the case where both components of the velocity are known the vorticity is calculated and it is used as a boundary condition to the transport equation. For the boundary points the tangential Eq. 13 or the normal Eq. 14 form should be employed. When both components of the velocity are known the tangent Eq. 13 form is used. When only one component is known, the normal Eq. 14 form is used. For interior points or for interfacial points where both components of the velocity are unknown the Eq. 12 is used. The discretized form of the integral Eq. 13 for a boundary collocation node $\mathbf{y}$ with respect to the region's interpolation nodal points $\mathbf{y}_k$ has the following form

$$
\begin{aligned}
&c(\mathbf{y})\mathbf{n}(\mathbf{y})\times\mathbf{u}(\mathbf{y})+\\
&\quad\mathbf{n}(\mathbf{y})\times\int_{\Gamma_{su}}\frac{\partial u^*}{\partial n}\begin{bmatrix}u_x\\u_y\\0\end{bmatrix}d\Gamma+\\
&\quad\mathbf{n}(\mathbf{y})\times\int_{\Gamma_s}\frac{\partial u^*}{\partial n}\Phi(\mathbf{y}_k)\,d\Gamma\begin{bmatrix}u_x\\u_y\\0\end{bmatrix}_{(\mathbf{y}_k)}+\\
&\quad\mathbf{n}(\mathbf{y})\times\int_{L_s}\frac{\partial u^*}{\partial n}\Phi(\mathbf{y}_k)\,d\Gamma\begin{bmatrix}u_x\\u_y\\0\end{bmatrix}_{(\mathbf{y}_k)}=\\
&\quad\mathbf{n}(\mathbf{y})\times\int_{\Gamma_{su}}\frac{\partial u^*}{\partial t}\begin{bmatrix}u_y\\-u_x\\0\end{bmatrix}d\Gamma+\\
&\quad\mathbf{n}(\mathbf{y})\times\int_{\Gamma_s}\frac{\partial u^*}{\partial t}\Phi(\mathbf{y}_k)\,d\Gamma\begin{bmatrix}u_y\\-u_x\\0\end{bmatrix}_{(\mathbf{y}_k)}+\\
&\quad\mathbf{n}(\mathbf{y})\times\int_{\Omega_s}\begin{bmatrix}-\frac{\partial u^*}{\partial y}\\\frac{\partial u^*}{\partial x}\\0\end{bmatrix}\Phi(\mathbf{y}_k)\,d\Omega[\omega]_{(\mathbf{y}_k)}.
\end{aligned}
\tag{40}
$$

Note that the integral envolving the gradient $\frac{\partial u^*}{\partial t}$ along the circular arc is always zero, since the vector $\mathbf{r}=\mathbf{y}-\mathbf{x}$ representing the distance between the source and the reference point is always perpendicular to the tangential vector $\mathbf{t}$. $u_x$ and $u_y$ are the cartesian components of the velocity field, defined either on the nodal point $\mathbf{y}$ or on the interpolating nodal points $\mathbf{y}_k$. The previous vector equation produces the following scalar equation

$$
\begin{aligned}
&c(\mathbf{y})n_x(\mathbf{y})u_y(\mathbf{y})\;-c(\mathbf{y})\;n_y(\mathbf{y})u_x(\mathbf{y})\;+\\
&\quad n_x(\mathbf{y})H^{\overline{u}_y}_{\Gamma_s}-n_y(\mathbf{y})H^{\overline{u}_x}_{\Gamma_s}+\\
&\quad n_x(\mathbf{y})H^k_{\Gamma_s}u_y(\mathbf{y}_k)-n_y(\mathbf{y})H^k_{\Gamma_s}u_x(\mathbf{y}_k)+\\
&\quad n_x(\mathbf{y})H^k_{L_s}u_y(\mathbf{y}_k)\;-n_y(\mathbf{y})H^k_{L_s}u_x(\mathbf{y}_k)\;=\\
&-n_x(\mathbf{y})T^{\overline{u}_x}_{\Gamma_s}-n_y(\mathbf{y})T^{\overline{u}_y}_{\Gamma_s}-\\
&\quad n_x(\mathbf{y})T^k_{\Gamma_s}u_x(\mathbf{y}_k)\;-n_y(\mathbf{y})T^k_{\Gamma_s}u_y(\mathbf{y}_k)\;+\\
&\quad\left[n_x(\mathbf{y})D^k_x+n_y(\mathbf{y})D^k_y\right]\omega(\mathbf{y}_k).
\end{aligned}
\tag{41}
$$

By applying the above equation for every boundary nodal point, where the vorticity is unknown, and imposing the boundary conditions accordingly, the tangential equation that corresponds to the nodal point $\mathbf{y}$ is derived. When one component of the velocity is unknown, the following discretized form of Eq. 14 is used for the boundary nodal point $\mathbf{y}$

$$
\begin{aligned}
&c(\mathbf{y})\mathbf{n}(\mathbf{y})\cdot\mathbf{u}(\mathbf{y})+\\
&\quad\mathbf{n}(\mathbf{y})\cdot\int_{\Gamma_{su}}\frac{\partial u^*}{\partial n}\begin{bmatrix}u_x\\u_y\end{bmatrix}d\Gamma+\\
&\quad\mathbf{n}(\mathbf{y})\cdot\int_{\Gamma_s}\frac{\partial u^*}{\partial n}\Phi(\mathbf{y}_k)\,d\Gamma\begin{bmatrix}u_x\\u_y\end{bmatrix}_{(\mathbf{y}_k)}+\\
&\quad\mathbf{n}(\mathbf{y})\cdot\int_{L_s}\frac{\partial u^*}{\partial n}\Phi(\mathbf{y}_k)\,d\Gamma\begin{bmatrix}u_x\\u_y\end{bmatrix}_{(\mathbf{y}_k)}=\\
&\quad\mathbf{n}(\mathbf{y})\cdot\int_{\Gamma_{su}}\frac{\partial u^*}{\partial t}\begin{bmatrix}u_y\\-u_x\end{bmatrix}d\Gamma+\\
&\quad\mathbf{n}(\mathbf{y})\cdot\int_{\Gamma_s}\frac{\partial u^*}{\partial t}\Phi(\mathbf{y}_k)\,d\Gamma\begin{bmatrix}u_y\\-u_x\end{bmatrix}_{(\mathbf{y}_k)}+\\
&\quad\mathbf{n}(\mathbf{y})\cdot\int_{\Omega_s}\begin{bmatrix}-\frac{\partial u^*}{\partial y}\\\frac{\partial u^*}{\partial x}\end{bmatrix}\Phi(\mathbf{y}_k)\,d\Omega[\omega]_{(\mathbf{y}_k)}.
\end{aligned}
\tag{42}
$$

which gives the following scalar equation

$$
\begin{aligned}
&c(\mathbf{y})n_x(\mathbf{y})u_x(\mathbf{y})+c(\mathbf{y})n_y(\mathbf{y})u_y(\mathbf{y})+\\
&\quad n_x(\mathbf{y})H^{\overline{u}_x}_{\Gamma_s}+n_y(\mathbf{y})H^{\overline{u}_y}_{\Gamma_s}+\\
&\quad n_x(\mathbf{y})H^k_{\Gamma_s}u_x(\mathbf{y}_k)+n_y(\mathbf{y})H^k_{\Gamma_s}u_y(\mathbf{y}_k)+\\
&\quad n_x(\mathbf{y})H^k_{L_s}u_x(\mathbf{y}_k)+n_y(\mathbf{y})H^k_{L_s}u_y(\mathbf{y}_k)=\\
&\quad n_x(\mathbf{y})T^{\overline{u}_y}_{\Gamma_s}-n_y(\mathbf{y})T^{\overline{u}_x}_{\Gamma_s}+\\
&\quad n_x(\mathbf{y})T^k_{\Gamma_s}u_y(\mathbf{y}_k)-n_y(\mathbf{y})T^k_{\Gamma_s}u_x(\mathbf{y}_k)+\\
&\quad \left[-n_x(\mathbf{y})D^k_y+n_y(\mathbf{y})D^k_x\right]\omega(\mathbf{y}_k)
\end{aligned}
\tag{43}
$$

This equation should be rearranged according to the boundary conditions. In case where both components of the velocity are unknowns the Eq. 12 is used. This equation is applied on interior and interfacial nodes

$$
\begin{aligned}
&\begin{bmatrix} u_x(\mathbf{y}) \\ u_y(\mathbf{y}) \end{bmatrix}+\int_{\Gamma_{su}}\frac{\partial u^*}{\partial n}\begin{bmatrix} u_x \\ u_y \end{bmatrix}d\Gamma+\\
&\qquad\int_{\Gamma_s}\frac{\partial u^*}{\partial n}\Phi(\mathbf{y}_k)\,d\Gamma\begin{bmatrix} u_x \\ u_y \end{bmatrix}_{(\mathbf{y}_k)}+\\
&\qquad\int_{L_s}\frac{\partial u^*}{\partial n}\Phi(\mathbf{y}_k)\,d\Gamma\begin{bmatrix} u_x \\ u_y \end{bmatrix}_{(\mathbf{y}_k)}=\\
&\qquad\int_{\Gamma_{su}}\frac{\partial u^*}{\partial t}\begin{bmatrix} u_y \\ -u_x \end{bmatrix}d\Gamma+\\
&\qquad\int_{\Gamma_s}\frac{\partial u^*}{\partial t}\Phi(\mathbf{y}_k)\,d\Gamma\begin{bmatrix} u_y \\ -u_x \end{bmatrix}_{(\mathbf{y}_k)}+\\
&\qquad\int_{\Omega_s}\begin{bmatrix} -\frac{\partial u^*}{\partial y} \\ \frac{\partial u^*}{\partial x} \end{bmatrix}\Phi(\mathbf{y}_k)\,d\Omega\,[\omega]_{(\mathbf{y}_k)}
\end{aligned}
\tag{44}
$$

and can be written in the vector form

$$
\begin{aligned}
&\begin{bmatrix} u_x(\mathbf{y}) \\ u_y(\mathbf{y}) \end{bmatrix}+\begin{bmatrix} H^{\overline{u}_x}_{\Gamma_s} \\ H^{\overline{u}_y}_{\Gamma_s} \end{bmatrix}+H^k_{\Gamma_s}\begin{bmatrix} u_x \\ u_y \end{bmatrix}_{(\mathbf{y}_k)}+\\
&H^k_{L_s}\begin{bmatrix} u_x \\ u_y \end{bmatrix}_{(\mathbf{y}_k)}=\begin{bmatrix} T^{\overline{u}_y}_{\Gamma_s} \\ -T^{\overline{u}_x}_{\Gamma_s} \end{bmatrix}+T^k_{\Gamma_s}\begin{bmatrix} u_y \\ -u_x \end{bmatrix}_{(\mathbf{y}_k)}+\\
&\qquad\qquad\begin{bmatrix} -D^k_y \\ D^k_x \end{bmatrix}[\omega]_{(\mathbf{y}_k)}.
\end{aligned}
\tag{45}
$$

This equation needs also to be rearranged according to the boundary conditions. In the above equation the vorticity is treated always as a body force. By combining Eq. 41, Eq. 43 and Eq. 45 the final system of equations $\mathbf{Ax}=\mathbf{b}$ is derived, which is in band form and is solved for the velocities and boundary vorticities. The involved boundary and volume integrals employed in the discretization of the kinematics integral equations are the following

$$H^{\overline{u}_x}_{\Gamma_s}=\int_{\Gamma^{u_x}_s}\frac{\partial u^*}{\partial n}\overline{u_x}\,d\Gamma \tag{46}$$

$$H^{\overline{u}_y}_{\Gamma_s}=\int_{\Gamma^{u_y}_s}\frac{\partial u^*}{\partial n}\overline{u_y}\,d\Gamma \tag{47}$$

$$H^k_{\Gamma_s}=\int_{\Gamma_s}\frac{\partial u^*}{\partial n}\Phi(\mathbf{y}_k)\,d\Gamma \tag{48}$$

$$H^k_{L_s}=\int_{L_s}\frac{\partial u^*}{\partial n}\Phi(\mathbf{y}_k)\,d\Gamma \tag{49}$$

$$T^{\overline{u}_x}_{\Gamma_s}=\int_{\Gamma^{u_x}_s}\frac{\partial u^*}{\partial t}\overline{u_x}\,d\Gamma \tag{50}$$

$$T^{\overline{u}_y}_{\Gamma_s}=\int_{\Gamma^{u_y}_s}\frac{\partial u^*}{\partial t}\overline{u_y}\,d\Gamma \tag{51}$$

$$T^k_{\Gamma_s}=\int_{\Gamma_s}\frac{\partial u^*}{\partial t}\Phi(\mathbf{y}_k)\,d\Gamma \tag{52}$$

and

$$D^k_j=\int_{\Omega_s}\frac{\partial u^*}{\partial x_j}\Phi(\mathbf{y}_k)\,d\Omega. \tag{53}$$

From Eq. 41 and Eq. 43 we deduce that the degree of freedom is equal to one, while the degrees of freedom of Eq. 45 are two. The following continuity condition should be applied on the interfacial nodal points, belonging to regions 1 and 2

$$\mathbf{u}|_1=\mathbf{u}|_2 \tag{54}$$

### *4.3 Kinetics integral equation*

Every region is discretized into a number of boundary elements $N_b$ and RBF cells $N_c$ as shown in Fig. 3 (b). By employing the boundary interpolation functions for the boundary elements and the

RBFs interpolations for cells the discretized form of the kinetics Eq. 22 is

$$c\omega(\mathbf{y})+\sum_{e=1}^{N_b}\int_{\Gamma_e}\frac{\partial p^*}{\partial n}N_e^k\,d\Gamma_e\,[\omega]_e^k= \sum_{e=1}^{N_b}\int_{\Gamma_e}p^*N_e^k\,d\Gamma_e\left[\frac{\partial\omega}{\partial n}\right]_e^k- \frac{1}{\nu}\sum_{e=1}^{N_b}\int_{\Gamma_e}p^*N_e^k\,d\Gamma_e\,[u_n]_e^k\,[\omega]_e^k+ \frac{1}{\nu}\sum_{c=1}^{N_c}\int_{\Omega_c}\frac{\partial p^*}{\partial x_j}N_c^k\,d\Omega_c\,[\tilde{u}_j]_c^k\,[\omega]_c^k+ \frac{1}{\nu\Delta t}\sum_{c=1}^{N_c}\int_{\Omega_c}p^*N_c^k\,d\Omega_c\,[\omega_{t-1}]_c^k \tag{55}$$

and in matrix form

$$c\omega+[Q]\,[\omega]=[P]\left[\frac{\partial\omega}{\partial n}\right]-\frac{1}{\nu}\,[P]\,[u_n]\,[\omega] +\frac{1}{\nu}\,[D_j]\,[u_j]\,[\omega]+\frac{1}{\nu\Delta t}\,[R]\,[\omega]_{t-1} \tag{56}$$

where

$$[Q]=\sum_{e=1}^{Nb}\int_{\Gamma_e}\frac{\partial p^*}{\partial n}\mathbf{N}_e\,d\Gamma_e \tag{57}$$

$$[P]=\sum_{e=1}^{Nb}\int_{\Gamma_e}p^*\mathbf{N}_e\,d\Gamma_e \tag{58}$$

$$[D_j]=\sum_{c=1}^{Nc}\int_{\Omega_c}\frac{\partial p^*}{\partial x_j}\mathbf{N}_c\,d\Omega_c \tag{59}$$

$$[R]=\sum_{c=1}^{Nc}\int_{\Omega_c}p^*\mathbf{N}_c\,d\Omega_c. \tag{60}$$

In the interface the following continuity conditions should be applied

$$\omega_1=\omega_2 \qquad \nu_1\left.\frac{\partial\omega}{\partial n}\right|_1=-\nu_2\left.\frac{\partial\omega}{\partial n}\right|_2. \tag{61}$$

By applying Eq. 56 to all nodal points and applying the continuity conditions Eq. 61 on the interface nodal points the following system of equations is obtained

$$\begin{bmatrix} K_1 & K_{12} & 0 & -P_1 & -P_{12} & 0 \\ 0 & K_{21} & K_2 & 0 & \frac{\nu_1}{\nu_2}P_{21} & -P_2 \end{bmatrix}\cdot \begin{bmatrix} \omega_1 \\ \omega_{12} \\ \omega_2 \\ \left.\frac{\partial\omega}{\partial n}\right|_1 \\ \left.\frac{\partial\omega}{\partial n}\right|_{12} \\ \left.\frac{\partial\omega}{\partial n}\right|_2 \end{bmatrix}=\mathbf{b} \tag{62}$$

where $P$ are the boundary integrals in Eq. 58. The index $_{12}$ denotes all interfacial boundary quantities on the first region and the index $_{21}$ denotes all interfacial boundary quantities on the second region. Finally in Eq. 62 the $[K]$ matrix is the following summation of integrals

$$[K]=[C]+[Q]+\frac{1}{\nu}\,[P]\,[u_n]-\frac{1}{\nu}\,[D_j]\,[u_j] \tag{63}$$

and $\mathbf{b}$ is the vector containing the internal products of the integrals and the boundary conditions

$$\mathbf{b}=\left\{-Q^k\overline{\omega}^k+P^k\overline{\frac{\partial\omega}{\partial n}}^k-\frac{1}{\nu}P^ku_n^k\overline{\omega}^k +\frac{1}{\nu}D_j^ku_j^k\overline{\omega}^k+\frac{1}{\nu\Delta t}R^k\overline{\omega}_{t-1}^k\right\} \tag{64}$$

With the multi-region technique the kinetics system of equations $\mathbf{A}\cdot\mathbf{x}=\mathbf{b}$ is in band form and special solvers can accelerate significantly the solution process.

### *4.4 Solution algorithm*

As it was already mentioned, two systems of equations must be solved in every iteration step. One system is related to the LBIE kinematics and the other to the BEM kinetics. With the optimal positioning of the coefficients, the systems can be stored in band form [Cuthill and McKee (1969)]. The time domain solution approach is the following.

- Discretize the domain into a number of regions and discretize every region into a number of points for the LBIE kinematics and

into a number of boundary and cell elements for the kinetics (Fig. 3).

- Evaluate the inverse local RBF matrix (Eq. 30) for every kinematics region and for every kinetics cell.
- Evaluate the integrals Eq. 48, Eq. 49 Eq. 52 and Eq. 53 for the kinematics.
- Start the time domain loop.
- Initialize the vorticity field.
- Start the iteration loop.
  - Evaluate the integrals Eq. 46, Eq. 47 Eq. 50 and Eq. 51 for the kinematics.
  - Form the kinematics system of equations Eq. 41, Eq. 43 and Eq. 45 and solve it for velocities and boundary vorticities.
  - Compute the constant part of the velocity $\overline{\mathbf{u}}$ in Eq. 16.
  - Compute kinetics integrals Eq. 57, Eq. 58 Eq. 59 and Eq. 60 when it is necessary.
  - Solve the transport equation Eq. 62 for vorticities and boundary vorticity fluxes.
  - Check convergence of the vorticity field and quit the iteration loop if it is achieved.
  - Relax vorticities and proceed to the next iteration step.
- End of iteration loop.
- End of time domain loop.

In the examples, the initial value for every time step is the vorticity field of the previous time step, and for the very first time step is equal to zero. The relaxation of the vorticity field is based on the following formula

$$\omega^{i+1} = \lambda\,\omega^{i} + (1-\lambda)\,\omega^{i-1} \tag{65}$$

where $0 < \lambda \leq 1$ is the relaxation parameter and $i$ denotes the iteration step.

The convergence norm of the problem is computed by the following formula

$$e = \frac{\sum_{j=1}^{N_t}\left(\omega_j^i - \omega_j^{i-1}\right)^2}{\sum_{j=1}^{N_t}\left(\omega_j^i\right)^2} \tag{66}$$

where the index $i$ denotes the iteration step and $j$ denotes the nodal point and $N_t$ denotes the total number of the kinetics nodal points. Each time the kinematics system is solved the constant part of the velocity Eq. 16 is computed for every region with the following formula

$$\overline{\mathbf{u}}_r = \frac{\sum_{i=1}^{N_r}\mathbf{u}_i}{N_r} \tag{67}$$

where $N_r$ is the total number of nodes and $\overline{\mathbf{u}}_r$ is the constant part of the decomposed velocity associated with the region $r$. The kinetics integrals for all regions are calculated at the first iteration of the initial time step. At the first iteration of the subsequent time steps the constant part of the velocity is calculated with Eq. 67 and if the perturbation exceeds a critical tolerance the kinetic integrals Eq. 57, Eq. 58, Eq. 59 and Eq. 60 are recomputed with the new mean constant velocity value. In the examples the tolerance for the kinetics recomputation is set to 0.01, the relaxation parameter $\lambda$ is equal to 0.1 and the convergence tolerance is $10^{-6}$.

## 5 Examples

### *5.1 Lid driven cavity*

The first problem concerns the well known lid driven cavity flow, widely used as a benchmark for incompressible flow codes. The fluid is contained in a squared unit cavity where the top wall moves with a constant velocity $\overline{u}_x = 1$ causing flow rotation (Fig. 5). The problem is solved with the proposed hybrid LBIE/BEM scheme for three different Reynolds numbers, Re = 400, Re = 1000 and Re = 3200. By taking into account the definition of the Reynolds number $Re = u_x L/\nu$ the viscosity coefficient $\nu$ is equal to 0.0025, 0.001 and 0.0003125 for the three test cases, respectively. The time step is 0.1 sec and the total number of steps are 500 for all cases. Mesh I (Fig. 6) is

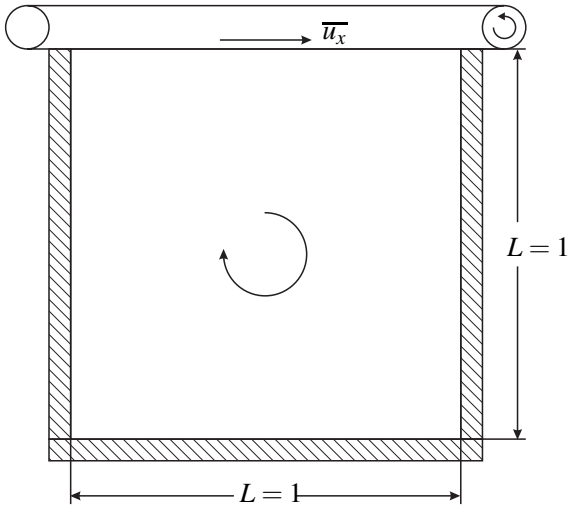


Figure 5: Lid driven cavity L × L.

used for Re = 400, while for Re = 1000 and Re = 3200 meshes II (Fig. 13) and III (Fig. 20) are adopted, respectively. In mesh I the cavity is discretized into 25x25 domains with ratio 1.15. The ratio is defined as the length of one element divided by the length of the previous one. In mesh II the cavity is discretized into 27x27 domains with ratio 1.1 and in mesh III the cavity is discretized into 41x41 domains with ratio 1.08. The radius of the nodal support domain is equal to 0.51 times the maximum side of the region where the node belongs. The variation of the horizontal component along a vertical line through the center of the cavity is depicted in Fig. 7, Fig. 14 and Fig. 21 for the three cases. Similarly the variation of the vertical component along a horizontal line through the center of the cavity is depicted in Fig. 8, Fig. 15 and Fig. 22. The vorticity on the moving wall boundary is shown in Fig. 9, Fig. 16 and Fig. 23. Moreover the distribution of the vorticity in the cavity is shown in the plots Fig. 10, Fig. 11, Fig. 17, Fig. 18 and Fig. 24, Fig. 25. Finally the postprocessed stream function is shown in Fig. 12, Fig. 19 and Fig. 26 for the three test cases. The results can be compared with the numerical results obtained by [Ghia, Ghia, and Shin (1982)].

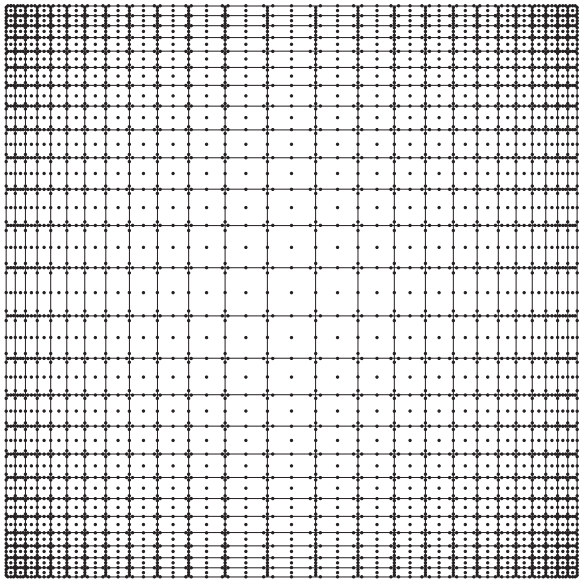

Figure 6: Mesh I of the cavity used for Re =400

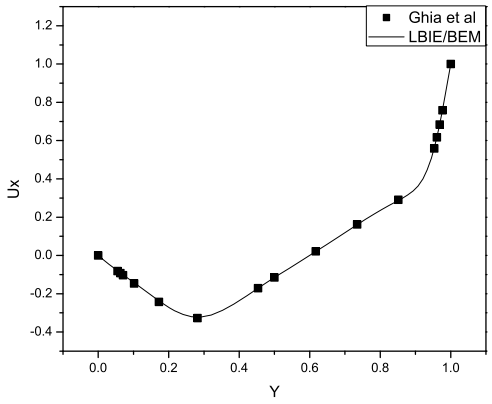


Figure 7: Profile of the velocity component $u_x$ along a vertical line through the center of the cavity (Re = 400).

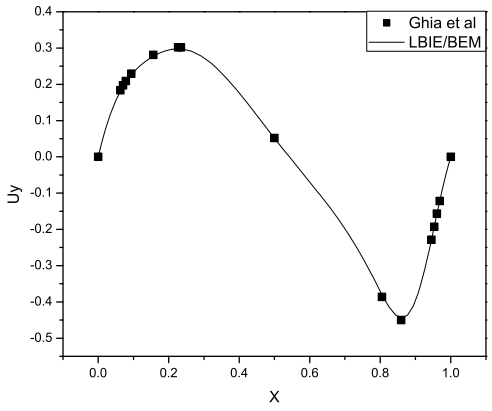


Figure 8: Profile of the velocity component $u_y$ along an horizontal line through the center of the cavity (Re = 400).

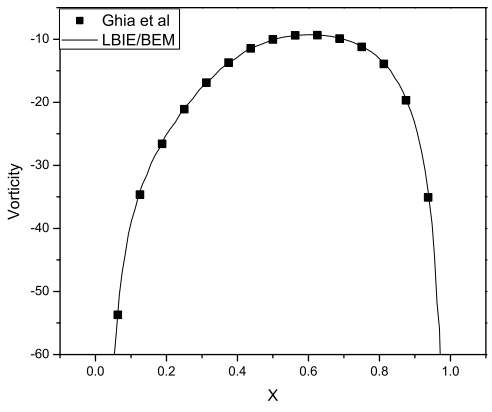


Figure 9: Vorticity at the moving wall of the cavity (Re = 400).

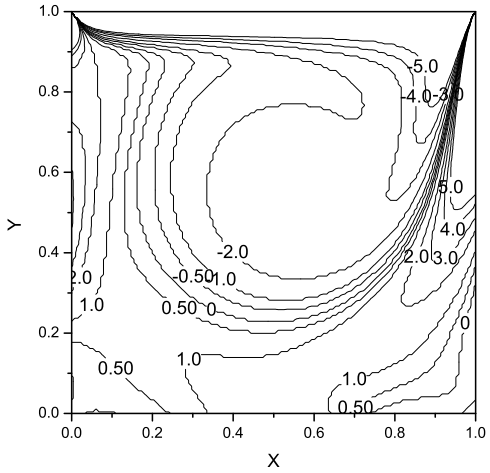


Figure 10: Vorticity distribution for the lid-driven cavity flow (Re=400)

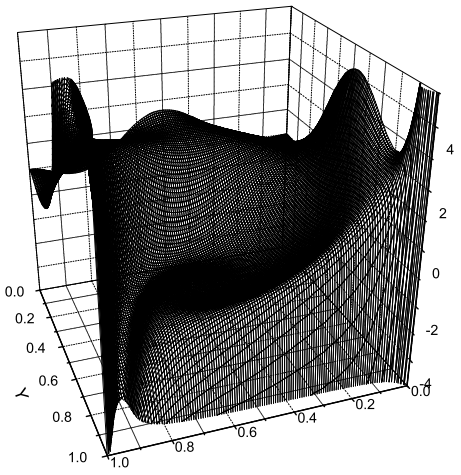


Figure 11: 3-D vorticity distribution for the lid-driven cavity flow (Re=400)

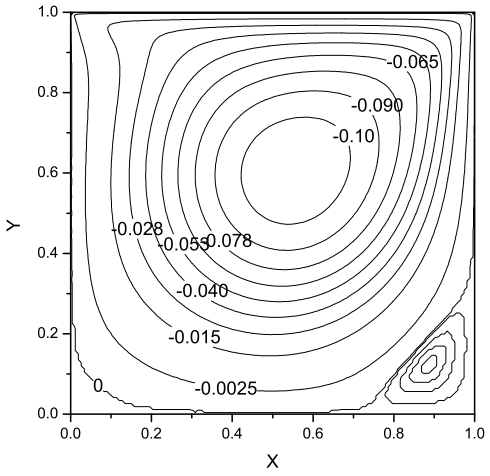


Figure 12: Streamlines for the lid-driven cavity flow (Re = 400)

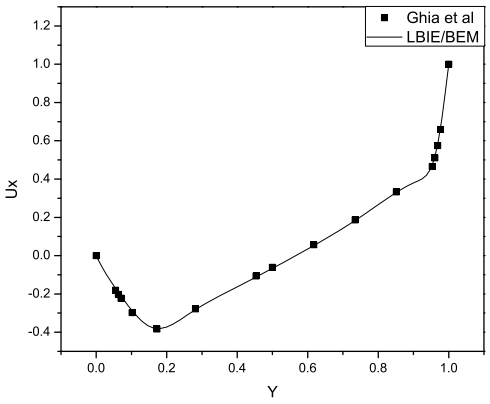


Figure 14: Profile of the velocity component $u_x$ along a vertical line through the center of the cavity (Re = 1000).

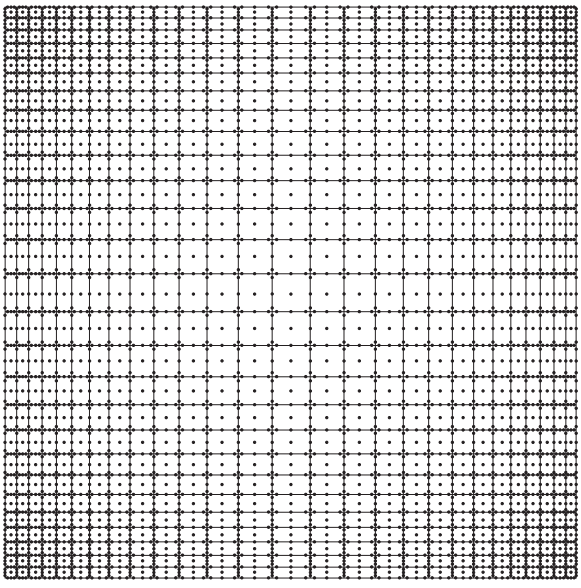

Figure 13: Mesh II of the cavity used for Re = 1000

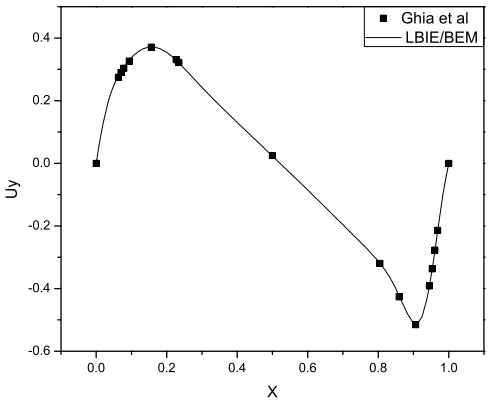


Figure 15: Profile of the velocity component $u_y$ along an horizontal line through the center of the cavity (Re = 1000).

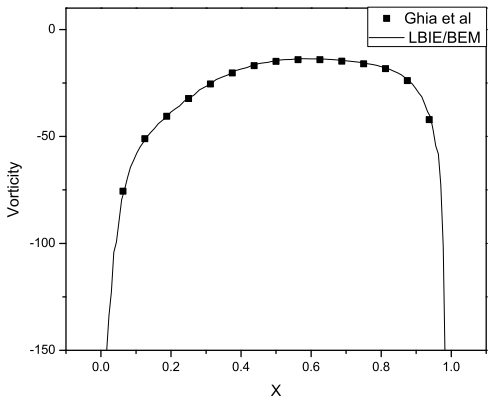


Figure 16: Vorticity at the moving wall of the cavity (Re = 1000).

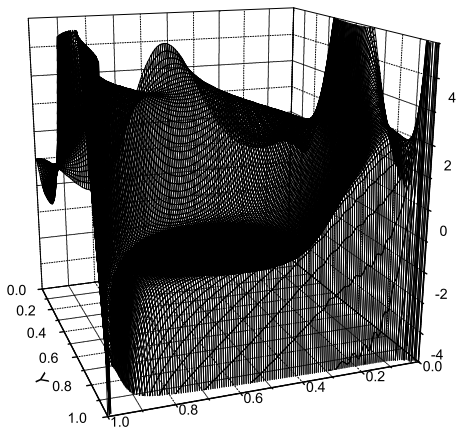


Figure 18: 3-D vorticity distribution for the lid-driven cavity flow (Re=1000)

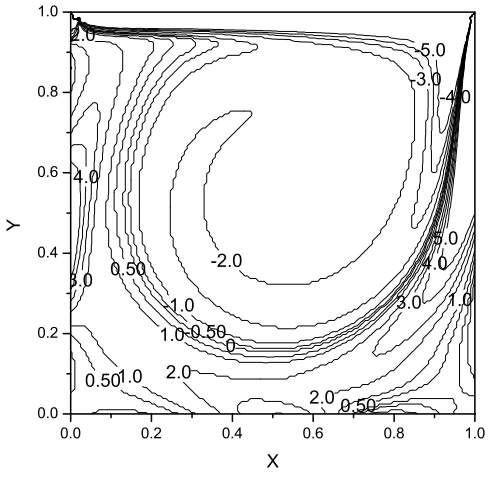


Figure 17: Vorticity distribution for the lid-driven cavity flow (Re=1000)

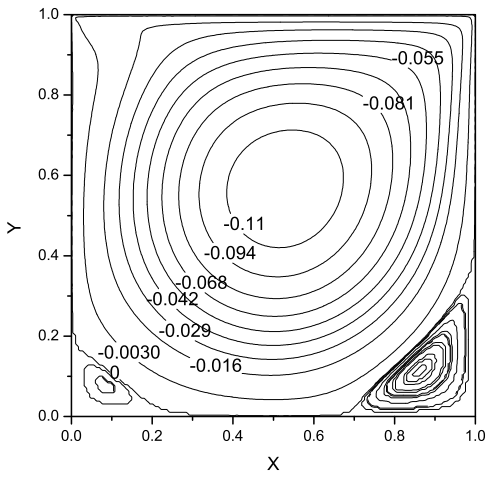


Figure 19: Streamlines for the lid-driven cavity flow (Re = 1000)

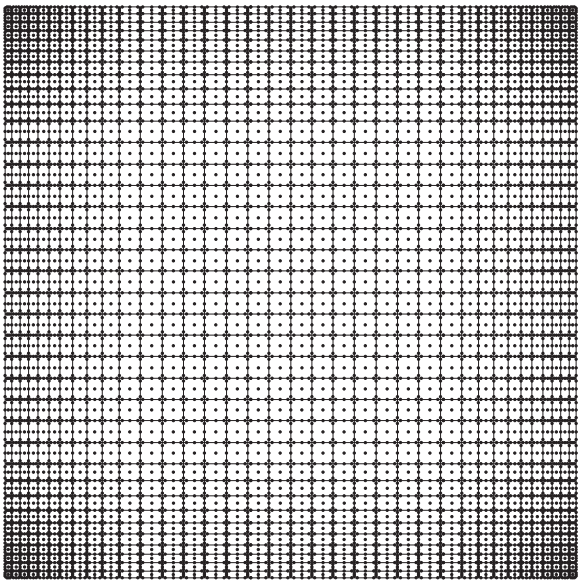

Figure 20: Mesh III of the cavity used for Re = 3200

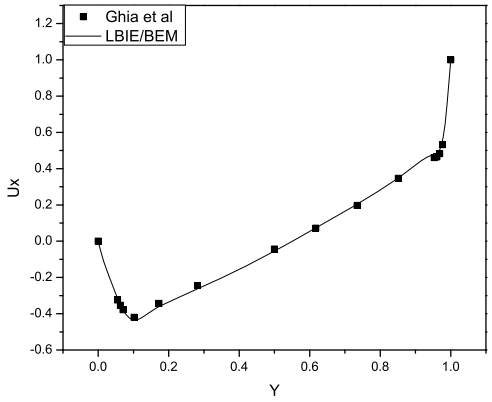


Figure 21: Profile of the velocity component $u_x$ along a vertical line through the center of the cavity (Re = 3200).

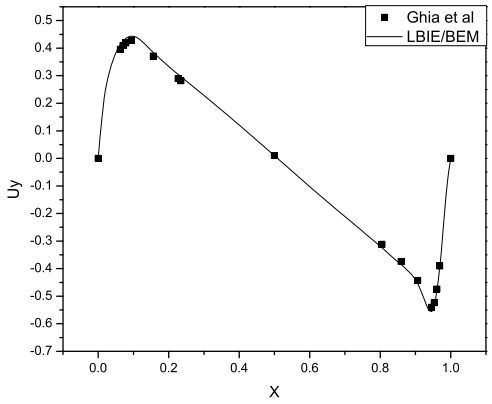


Figure 22: Profile of the velocity component $u_y$ along an horizontal line through the center of the cavity (Re = 3200).

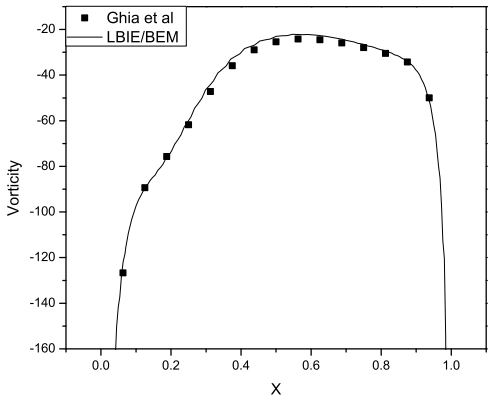


Figure 23: Vorticity at the moving wall of the cavity (Re = 3200).

### *5.2 L-shape cavity*

The second example concerns the L shaped cavity as it is described in [Hribersek and Skerget (2005)]. The length and the height of the domain is equal to $L = 1$ (Fig. 27), the diffusion coefficient is equal to $\nu = 0.001$ and the top wall is moving with velocity $u_x = 1$, resulting the Reylonds number 1000. The domain is discretized into 1200 domains with ratio 1.1 as shown in Fig. 28. The considered time step is 0.1 and the problem is studied for 500 time steps. In Fig. 29 is depicted the variation of the $u_x$ component on the vertical line through the position $x = 0.75$. In Fig. 30 is shown the variation of the $u_y$ along an horizontal line through the horizontal position

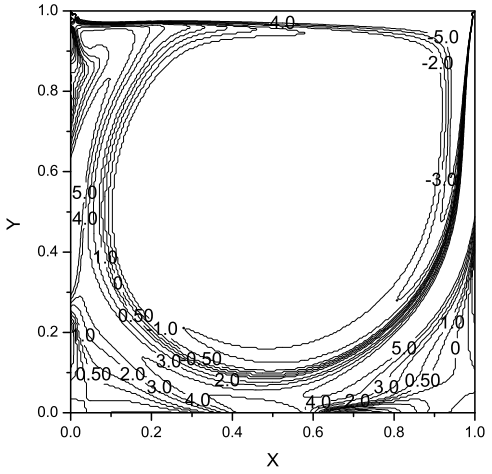


Figure 24: Vorticity distribution for the lid-driven cavity flow (Re=3200)

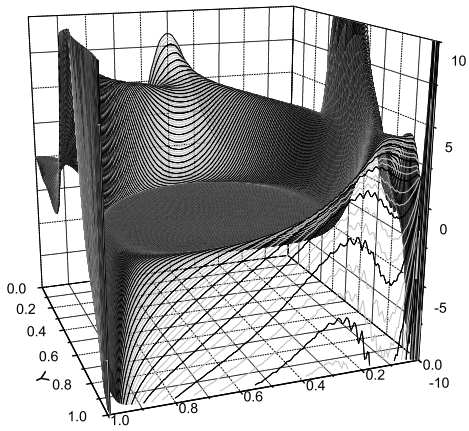


Figure 25: 3-D vorticity distribution for the lid-driven cavity flow (Re=3200)

$y = 0.75$. Finally on Fig. 31 the vorticity isolines are plotted.

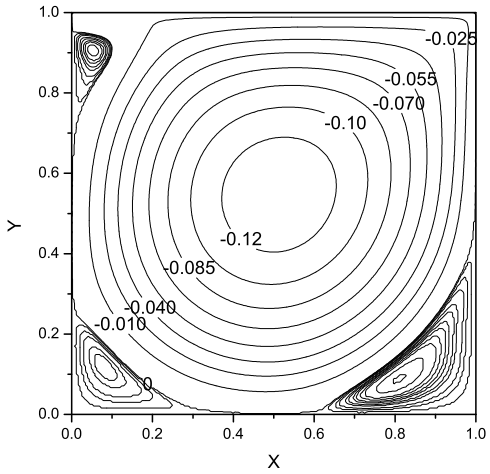


Figure 26: Streamlines for the lid-driven cavity flow (Re = 3200)

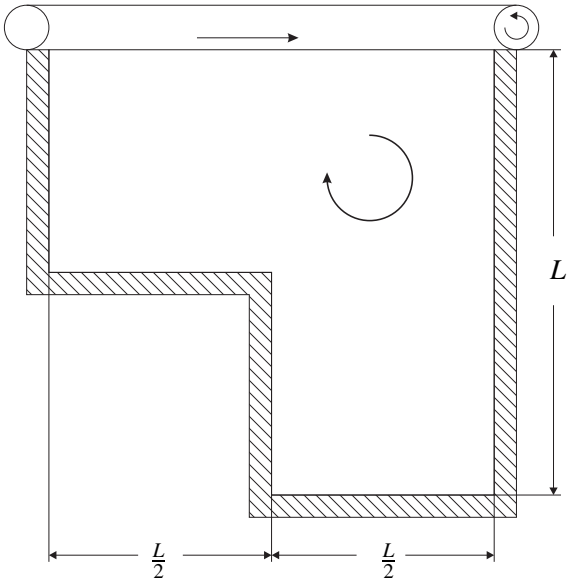


Figure 27: L-cavity problem description.

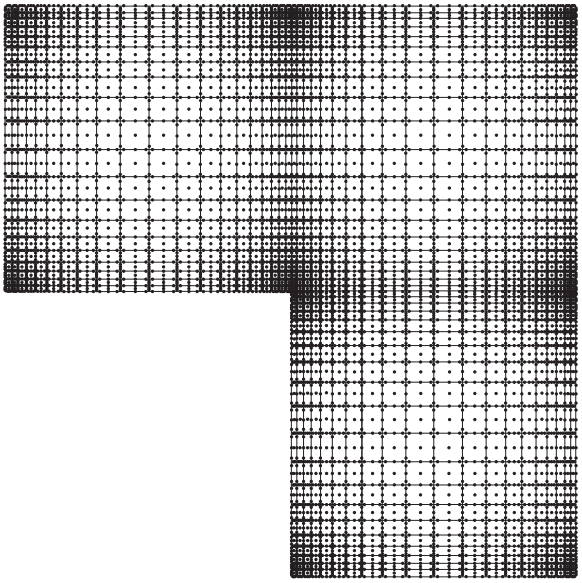

Figure 28: Discretization of the L-cavity.

### 5.3 Backward facing step

The third example concerns the backward facing step channel as shown in Fig. 32. The problem is solved for Reynolds number 200. The height of the channel is $H = 1$, the length of the step is $L_s = 1$ and the length of the channel is $L = 9$. The

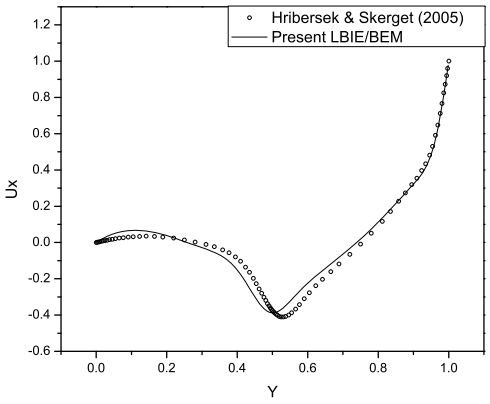


Figure 29: Profile of the velocity component $u_x$ along a vertical line through the x=0.75 of the L-cavity.

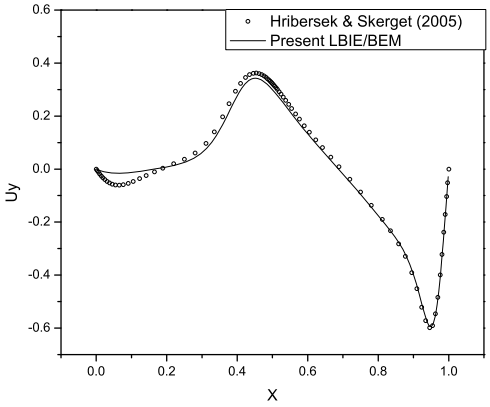


Figure 30: Profile of the velocity component $u_y$ along an horizontal line through the y=0.75 of the L-cavity.

Reynolds number is defined as $Re = \frac{\overline{u}H}{\nu}$, where $\overline{u}$ is the average velocity at the inflow boundary. The $u_x$ component of the velocity on the left side of the channel has the following form

$$u(y) = \begin{cases} 1 - \left(\frac{y-0.75}{0.25}\right)^2 & y > 0.5 \\ 0 & y \leq 0.5 \end{cases} \tag{68}$$

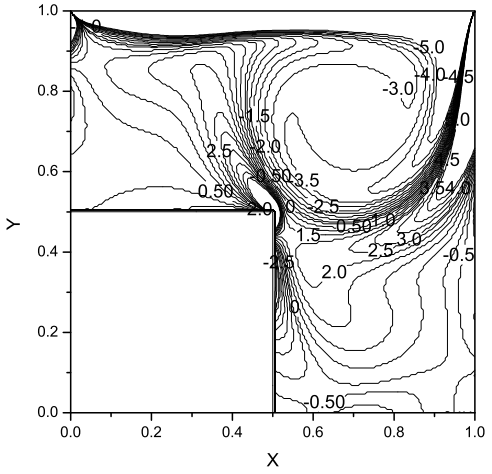


Figure 31: Vorticity distribution in the L-cavity.

while $u_y = 0$. At the step, the top and the low wall of the channel both velocity components have zero values $u_x = 0$ and $u_y = 0$ while at the outlet $u_y = 0$ and the $u_x$ is unknown. For the kinetics the outflow boundary is prescribed with vanishing boundary vorticity flux ($\frac{\partial \omega}{\partial n} = 0$). The channel is discretized into 760 regions as it is shown in Fig. 33. The density of the discretization is 80 regions in $x$ direction and 10 regions in $y$ direction. The nodal support domain is selected to be 0.51 of the maximum region's side where the node belongs. The considered time step is equal to 0.5 sec and the problem is studied for 250 time steps. The outflow percentage is equal to 98.8%, showing that the incompresibility criterion is sufficiently satisfied. The circulation length is computed to be 2.68 and it is compared with the value 2.656 of [Zhang (2005)]. In Fig. 34 the $u_x$ profile of the velocity is depicted in various positions in the channel. The distribution of the vorticity is shown in Fig. 35 and finally in Fig. 36 represents the streamlines in the recirculation area.

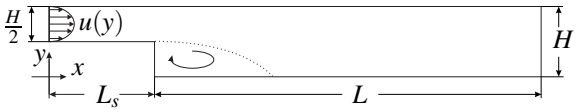


Figure 32: Backward facing step geometry

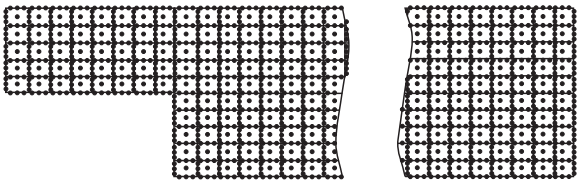

Figure 33: Backward facing step discretization

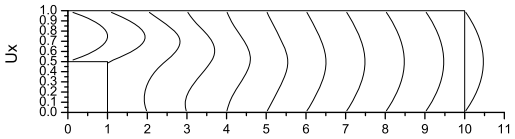


Figure 34: Profiles of the velocity $u_x$ component in various positions of the channel.

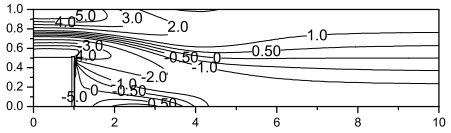

Figure 35: Vorticity distribution

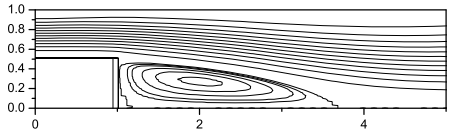

Figure 36: Streamlines in the recirculation area

## 6 Conclusions

In the present work a hybrid multi-region velocity-vorticity computational scheme for the solution of the 2D Navier-Stokes equations is presented. The domain is divided into a number of regions and every region is associated with a lo-

cal RBF matrix for the kinematics equations. The RBF interpolation of the velocity field is guaranteed to be continuous in the entire region. Numerical examples show that the presence of the interfaces improve stability and accuracy and ensures the continuity of the velocity field in the whole domain. For the solution of the transport kinetics a parabolic-diffusion boundary-domain integral equation is involved and solved by the BEM. Special discontinuous RBF cells are used for the interpolation of the vorticity. The decomposition of the convective velocity into a constant and a variable part results on a very stable and accurate upwind scheme for the vorticity transport equation.

**Acknowledgement:** This work has been supported by the Research Project PTDC/MAT/68166/2006, the Center of Mathematics and its Applications (CEMAT) through FCT's Funding Program and by the grant SFRH / BPD / 27225 / 2006 of FCT (E.J.Sellountos).

## References

**Alujevic, A.; Kuhn, G.; Skerget, P.** (1991): Boundary elements for the solution of Navier-Stokes equations. *Comput Meth Appl Mech Engrg*, vol. 91, no. 1-3, pp. 1187–1201.

**Atluri, S.; Shen, S.** (2002): The meshless local Petrov-Galerkin (MLPG) method: A simple and less-costly alternative to the finite and boundary element method. *Comp Meth Appl Mech Engrg*, vol. 3, no. 1, pp. 11–51.

**Bokota, A.; Iskierka, S.** (1995): An analysis of the diffusion-convection problem by the boundary element method. *Engng An Bound Elem*, vol. 15, pp. 267–275.

**Cheng, M.; Liu, G. R.** (2002): A novel finite point method for flow simulation. *Int J Num Meth Fluids*, vol. 39, no. 12, pp. 1161–1178.

**Cuthill, E.; McKee, J.** (1969): Reducing the bandwidth of sparse symmetric matrices. *Proc 24th Nat Conf ACM*, pp. 157–172.

**Ghia, U.; Ghia, K.; Shin, C.** (1982): High-Re solutions for incompressible flow using the Navier-Stokes equations and a multigrid method. *J. Comput. Physics*, vol. 48, pp. 387–411.

**Guj, G.; Stella, F.** (1993): A vorticity-velocity method for the numerical solution of 3D incompressible flows. *J Comput Phys*, vol. 106, pp. 286–298.

**Hardy, R.** (1990): Theory and applications of the multiquadrics-biharmonic method (20 years of discovery 1968–1988). *Comput and Math with Appl*, vol. 19, pp. 163–208.

**Hribersek, M.; Skerget, L.** (1998): Iterative methods in solving Navier-Stokes equations by the boundary element method. *Int J Num Meth Engrg*, vol. 39, no. 1, pp. 115–139.

**Hribersek, M.; Skerget, L.** (2005): Boundary domain integral method for high Reynolds viscous fluid flows in complex planar geometries. *Comp Meth Appl Mech Engrg*, vol. 194, pp. 4196–4220.

**Li, J.; Hon, Y.; Chen, C.** (2002): Numerical comparisons of two meshless methods using radial basis functions. *Engng An Bound Elem*, vol. 26, pp. 205–225.

**Lin, H.; Atluri, S. N.** (2001): The meshless Local Petrov-Galerkin (MLPG) method for solving incompressible Navier-Stokes equations. *CMES: Computer Modeling in Engineering & Sciences*, vol. 2, no. 2, pp. 117–142.

**Liu, C. H.** (2001): Numerical solution of three-dimensional Navier-Stokes equations by a velocity-vorticity method. *Int J Num Meth Fluids*, vol. 35, no. 5, pp. 533–557.

**Liu, G.; Gu, Y.; Dai, K.** (2004): Assessment and applications of point interpolation methods for computational mechanics. *Intern J Num Meth Engrg*, vol. 59, no. 10, pp. 1373–1397.

**Nicolás, A.; Bermúdez, B.** (2007): Viscous incompressible flows by the velocity-vorticity Navier-Stokes equations. *CMES: Computer Modeling in Engineering & Sciences*, vol. 20, no. 2, pp. 73–83.

**Onate, E.; Idelsohn, S.; Zienkiewicz, O. C.; Taylor, R. L.** (1998): A Finite Point Method in Computational Mechanics. Applications to Convective Transport and Fluid Flow. *Int J Num Meth Engrng*, vol. 39, no. 22, pp. 3839–3866.

**Sellountos, E.; Sequeira, A.** (2007): An advanced meshless LBIE/RBF method for solving two dimensional incompressible fluid flows . *Comp Mech (to appear)*.

**Sellountos, E. J.; Polyzos, D.** (2003): A MLPG (LBIE) method for solving frequency domain elastic problems. *CMES: Computer Modeling in Engineering & Sciences*, vol. 4, no. 6, pp. 619–636.

**Sellountos, E. J.; Polyzos, D.** (2005): A MLPG(LBIE) approach in combination with BEM. *Comp Meth Appl Mech Engrg*, vol. 194, no. 6-8, pp. 859–875.

**Shu, C.; Ding, H.; Yeo, K.** (2005): Computation of Incompressible Navier-Stokes Equations by Local RBF-based Differential Quadrature Method. *CMES: Computer Modeling in Engineering & Sciences*, vol. 7, no. 2, pp. 195–205.

**Skerget, L.; Hribersek, M.; Zunic, Z.** (2003): Natural convection flows in complex cavities by BEM. *Int J Numer Meth Heat Fluid*, vol. 13, no. 5/6, pp. 720–736.

**Skerget, L.; Rek, Z.** (1995): Boundary-domain integral method using a velocity-vorticity formulation. *Engrg An Boundary Elements*, vol. 15, no. 4, pp. 359–370.

**Tsai, C.; Young, D.; Cheng, A.-D.** (2002): Meshless BEM for Three-dimensional Stokes Flows. *CMES: Computer Modeling in Engineering & Sciences*, vol. 3, no. 1, pp. 117–128.

**Wang, J.; Liu, G.** (2002): A point interpolation meshless method based on radial basis functions. *Int J Numer Meth Engng*, vol. 54, pp. 1623–1648.

**Wang, J.; Liu, G.** (2002): On the optimal shape parameters of radial basis functions used for 2-D meshless methods. *Comp Meth Appl Mech Engrg*, vol. 191, no. 23-24, pp. 2611–2630.

**Wu, N.-J.; Tsay, T.-K.; Young, D. L.** (2005): Meshless numerical simulation for fully nonlinear water waves. *Int J Num Meth Fluids*, vol. 50, no. 2, pp. 219–234.

**Zhang, K. K.** (2005): A discrete splitting finite element method for numerical simulations of incompressible Navier-Stokes flows. *Int J Num Meth Engng*, vol. 64, no. 3, pp. 285–303.

**Zhu, B.** (2005): Finite volume solution of the Navier-Stokes equations in velocity-vorticity formulation. *Int J Num Meth Fluids*, vol. 48, no. 6, pp. 607–629.

**Zienkiewicz, O.; Taylor, R.** (2000): *The Finite Element Method. Volume 3: Fluid Mechanics 5fth Ed.* B-H Oxford UK.

**Zunic, Z.; Hribersek, M.; Skerget, L.; Ravnik, J.** (2007): 3-D boundary element-finite element method for velocity-vorticity formulation of the Navier-Stokes equations. *Engrg An Boundary Elements*, vol. 31, no. 3, pp. 259–266.